Quantum Capacitance Estimations of Pyrrolic Rich Graphene for Supercapacitor Electrodes

Article *in* IEEE Transactions on Nanotechnology · December 2017

DOI: 10.1109/TNANO.2017.2786715

CITATIONS
14

READS
279

4 authors:

Boddepalli Santhibhushan
Indian Institute of Information Technology Allahabad
35 PUBLICATIONS **350** CITATIONS
SEE PROFILE

Md. Shahzad Khan
Galgotias University
56 PUBLICATIONS **497** CITATIONS
SEE PROFILE

Vijay Kumar Bohat
Netaji Subhas University of Technology
15 PUBLICATIONS **416** CITATIONS
SEE PROFILE

Anurag Srivastava
ABV-Indian Institute of Information Technology and Management Gwalior
263 PUBLICATIONS **2,248** CITATIONS
SEE PROFILE

IEEE Transactions on Nanotechnology, DOI: 10.1109/TNANO.2017.2786715

Quantum Capacitance Estimations of Pyrrolic Rich Graphene for Supercapacitor Electrodes

Boddepalli SanthiBhushan, *Student Member, IEEE*, Mohammad Shahzad Khan, Vijay Kumar Bohat, *Student Member, IEEE*, Anurag Srivastava*, *Member, IEEE*

***Abstract*- Despite having remarkable surface area (2630 m^2/g for graphene), the graphene based supercapacitors still unable to attain the necessary energy density due to poor accessibility of surface area and low quantum capacitance. In this work, we demonstrate an effective way to improve the quantum capacitance of graphene through plane wave Density Functional Theory (DFT) calculations. We used pyrrolic type nitrogen doping to demonstrate extremely high quantum capacitances for graphene. An impressive 486.32 uF/cm^2 quantum capacitance has been observed at a pyrrolic concentration of 6.38%. Our calculations suggest that, the quantum capacitance of graphene increases with the pyrrolic concentration. We have also investigated the impact of combinational pyrrolic defects on the quantum capacitance of graphene. We believe that, the pyrrolic defects studied in this work also help in improving the graphene surface area accessibility by the electrolytic ions.**

***Index Terms* – Supercapacitor, Graphene, Quantum Capacitance, Plane wave DFT, Defects.**

I. INTRODUCTION

As the world is focusing more on increasing the renewal energy production and zero-emission fuels in order to cut the green house emissions, the need for sophisticated energy storage devices is also increasing. Hydrogen fuel, being a non-emission fuel is been widely explored by the researchers around the globe for means to store and use efficiently [1-3]. The dependence on renewal energy highlights the need for high energy density storage devices as this form of energy cannot be produced uniformly with time. For instance, it is not possible to produce solar power during night; the wind and tidal powers are dependent on Mother Nature. In addition, there is a great need for sophisticated regenerative energy storage devices to store and effectively use the intermittent energy released in several applications. Supercapacitor is one such a promising device with its ability of extremely fast charging and discharging (high power density) and extremely high life time (> 10000 cycles). However, the supercapacitor offers relatively low energy density (5-10 Wh/kg) in comparison to conventional storage devices lead-acid battery (20-35 Wh/kg), Li-ion battery (120-170 Wh/kg), LiMH battery (40-100 Wh/kg) [4-8]. Graphene is the most promising alternative to the conventional supercapacitor electrode material, activated carbon, due to its extremely large surface area, high conductivity, mechanical robustness and stability. Nevertheless, the predicted upper limit of double layer capacitance for graphene supercapacitors (C_{DL} ~ 550 F/g) could not be attained due to the poor accessibility of graphene's large surface area by the electrolytic ions. Reason being, the agglomeration of graphene sheets during their synthesis from graphene oxide leading to poor volumetric specific area [9-10].

B. SanthiBhushan, V. K. Bohat and A. Srivastava are with the Computational Nanoscience and Technology Laboratory, Advanced Materials Research Group, Atal Bihari Vajpayee–Indian Institute of Information Technology and Management, Gwalior 474010, India (e-mail: bsb8897@gmail.com; vijay.bohat@gmail.com; profanurag@gmail.com). * corresponding author.

M. S. Khan is with Department of Physics, Michigan Technological University, Houghton, MI 49931, USA (e-mail: kshahzad001@gmail.com).

Several reports predicted that, introducing defects and doping onto graphene improves the effective surface area accessible by the electrolytic ions and the quantum capacitance (C_Q) of graphene [11-16]. The quantum capacitance is an intrinsic capacitance offered by the materials having limited density of states at Fermi level. The total capacitance (C_T) that dictates the energy density of supercapacitor is a dependent quantity of double layer and quantum capacitances ($\frac{1}{C_T} = \frac{1}{C_Q} + \frac{1}{C_{DL}}$). Thus, it is mandatory to use electrode materials with sufficiently large quantum capacitance to obtain high energy densities. In this work, we computationally report pyrrolic rich graphenes for enhanced quantum capacitances and improved surface area accessibility. Earlier, our group has predicted the pyrrolic defect as more favourable than pyridinic and graphitic defects based on DOS profiles [9]. In this work, we verified the same through quantum capacitance calculations. Further, we explored the impact of increasing pyrrolic concentration on quantum capacitance of graphene sheet, and the influence of other defects such as Stone-Wales, graphitic and pyridinic on the quantum capacitance of pyrrolic graphene.

II. COMPUTATIONAL DETAILS

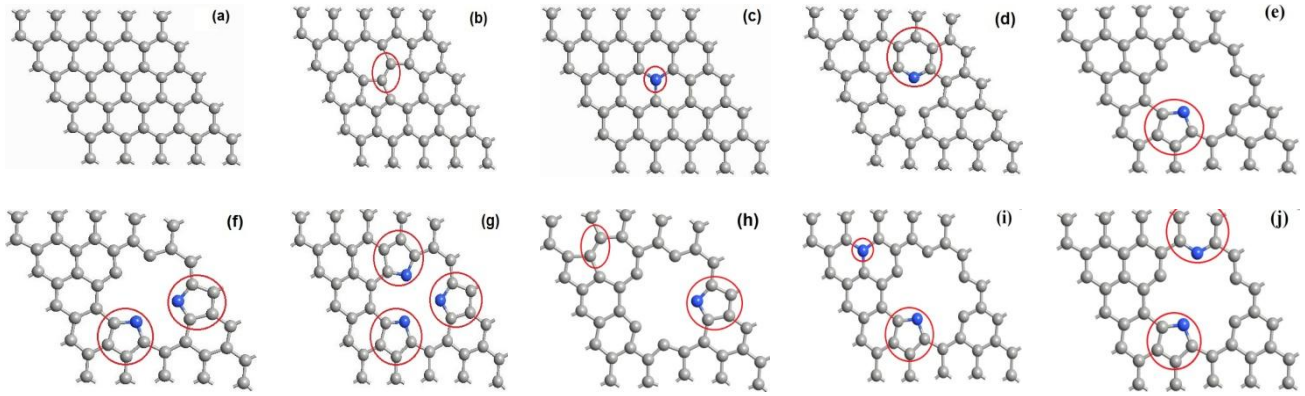

Fig. 1. Different graphene defect configurations studied, (a) Pristine Graphene, (b) Stone-Wales, (c) Graphitic, (d) Pyridinic, (e) Pyrrolic, (f) 2N-Pyrrolic, (g) 3N-Pyrrolic, (h) Pyrrolic+Stone-Wales, (i) Pyrrolic+Graphitic, (j) Pyrrolic+Pyridinic. (b-e) are different primary defects, (e-g) are defects with increasing pyrrolic concentration, (h-j) are combinational pyrrolic defects. (The defect sites are circled red. The grey and blue balls indicate carbon and nitrogen atoms, respectively.)

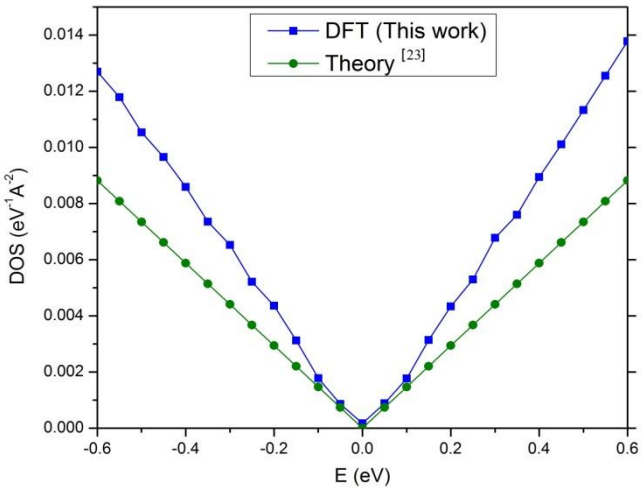

Fig. 2. Comparison of DOS per unit area of pristine graphene from DFT (this work) and Theory [23].

The present calculations are performed through plane wave Density Functional Theory formalism (DFT) as implemented in Quantum ESPRESSO package [17]. We used ultrasoft pseudopotentials [18] to describe the interaction between nuclei and electrons. The Perdew-Burke-Ernzerhof (PBE) functional [19] within the Generalized Gradient Approximation (GGA) was employed to describe the exchange-correlation interaction energy of electrons. Kohn-Sham wave functions were represented by a plane-wave basis with an energy cutoff of 30 Ry and charge density with a cutoff of 300 Ry. All the defect configurations are realized on a 5*5 hexagonal supercell (50 atoms) of graphene. Sufficient vacuum of 15 Å has been considered in the orthogonal direction of graphene sheet to avoid inter-layer interaction. The Brillouin zone has been sampled with 6*6*1 Monkhorst-Pack grid of k-points, while the DOS profiles extracted with 27*27*1 k-points. To aid the K-point convergence, Marzari-Vanderbilt smearing [20] of 0.005 Ry has been applied.

III. RESULTS AND DISCUSSION

The present work reports quantum capacitance estimations of pyrrolic rich graphene configurations along with their structural stability and electronic nature. The work has been devided into three parts, (A) comparative analysis of different primary defects (shown in Fig. 1(b-e)) for identifying the most favorable defect, (B) analyzing the influence of pyrrolic concentration (Fig. 1(e-g)), and (C) analyzing the impact of other defects on pyrrolic graphene (Fig. 1(h-j)).

A. Primary Defects

The pristine graphene sheet (Fig.1(a)) has been subjected to different possible primary defects namely Stone-Wales, Graphitic, Pyridinic and Pyrrolic as shown in Fig. 1(b-e). The structural parameters such as C-C bond lengths, C-N bond lengths and formation energies are listed in table I. The observed C-C bond length of pristine graphene (1.42 Å) is in excellent agreement with the experimental reports [21, 22]. Considerable variations in the bond lengths of graphene have been witnessed as the sheets are subjected to Stone-Wales and Nitrogen based defects. The thermodynamic stability is an important factor that can give a comparative idea about the life times of defect configurations as supercapacitor electrodes. The thermodynamic stability for our defect configurations has been assessed through calculation of formation energies per unit length of sheet (E_F^L), through the expression given in eq-(1) [15].

$$E_F^L = \frac{[E_D - xE_C - y\frac{E_{N_2}}{2}]}{L} \quad \text{- (1)}$$

Here, E_D, E_C and E_{N_2} refer to the energies of defected sheet, carbon atom of pristine graphene, and nitrogen gas, respectively. x and y indicate the number of carbons and nitrogens present in the defect configuration. L is the length

TABLE I
STRUCTURAL AND ELECTRONIC PROPERTIES OF DIFFERENT DEFECT CONFIGURATIONS (HERE, C AND N REFER TO CARBON AND NITROGEN, RESPECTIVELY.)

Defect Type	C-C Bond Length (Å)	C-N Bond Length (Å)	Formation Energy E_F^L (eV/Å)	Electronic Nature	Peak C_Q (uF/cm^2)
Graphene	1.420	-	-	Zero Band Gap	22.17
Stone-Wales	1.331-1.482	-	0.34	Semi metallic	110.85
Graphitic	1.415-1.425	1.408	0.06	Metallic	123.77
Pyridinic	1.395-1.520	1.317	0.42	Metallic	91.40
Pyrrolic	1.383-1.459	1.393	1.21	Metallic	195.12
2N Pyrrolic	1.384-1.471	1.378-1.396	0.94	Metallic	251.56
3N Pyrrolic	1.367-1.458	1.383	0.69	Metallic	486.32
Pyrrolic + Stone-Wales	1.347-1.540	1.409-1.413	1.47	Metallic	215.55
Pyrrolic + Graphitic	1.385-1.473	1.383-1.417	1.23	Metallic	180.40
Pyrrolic + Pyridinic	1.369-1.460	1.335-1.401	1.06	Metallic	209.71

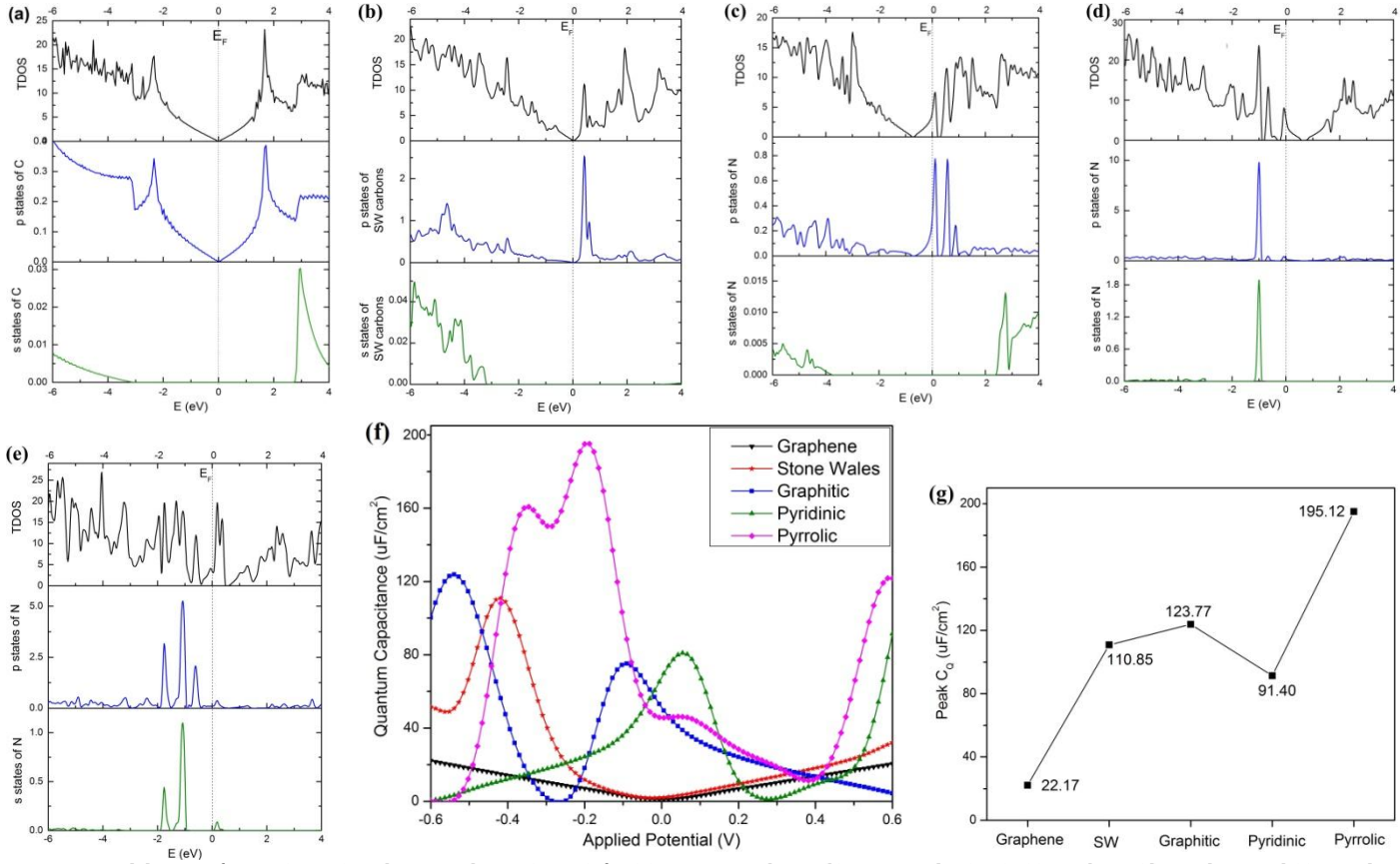

Fig. 3. Total density of states (TDOS) and Projected DOS (PDOS) for (a) pristine graphene, (b) Stone-Wales (SW), (c) graphitic, (d) pyridinic, and (e) pyrrolic defected graphenes (Fermi level (E_F) is located at energy zero, DOS are in the units of eV^{-1}). (f) Quantum Capacitance plotted as a function of applied potential for different primary defects, (g) peak value of quantum capacitance for different primary defects.

of the sheets considered (~12.30 Å). The calculated formation energies are listed in table I, where the defect with low formation energy is considered relatively more stable than its counterparts. The graphitic configuration is observed to be most stable among the defect configurations studied, owing to its least formation energy. The stability of the primary defects is observed to follow the pattern graphitic > Stone-Wales > pyridinic > Pyrrolic. By definition, the positive sign against the formation energies refer to endothermic process of defect creation where energy is consumed during the process; while the negative sign (if any) refer to exothermic process where energy is released. The formation energies of all our defects are positive, predicting the endothermic nature of their creation.

The electronic nature of pristine graphene and its primary defect configurations are predicted through Total density of states (TDOS) and Projected DOS (PDOS) calculations. Before proceeding further to the TDOS and PDOS calculations of defected configurations, we have evaluated our DFT based TDOS for pristine graphene with that of theory. For pristine graphene, the TDOS (D(E)) near Dirac point can be approximated by the mathematical expression [23],

$$D(E) \approx \frac{g_s g_v}{2\pi(\hbar v_F)^2}|E| \qquad \text{- (2)}$$

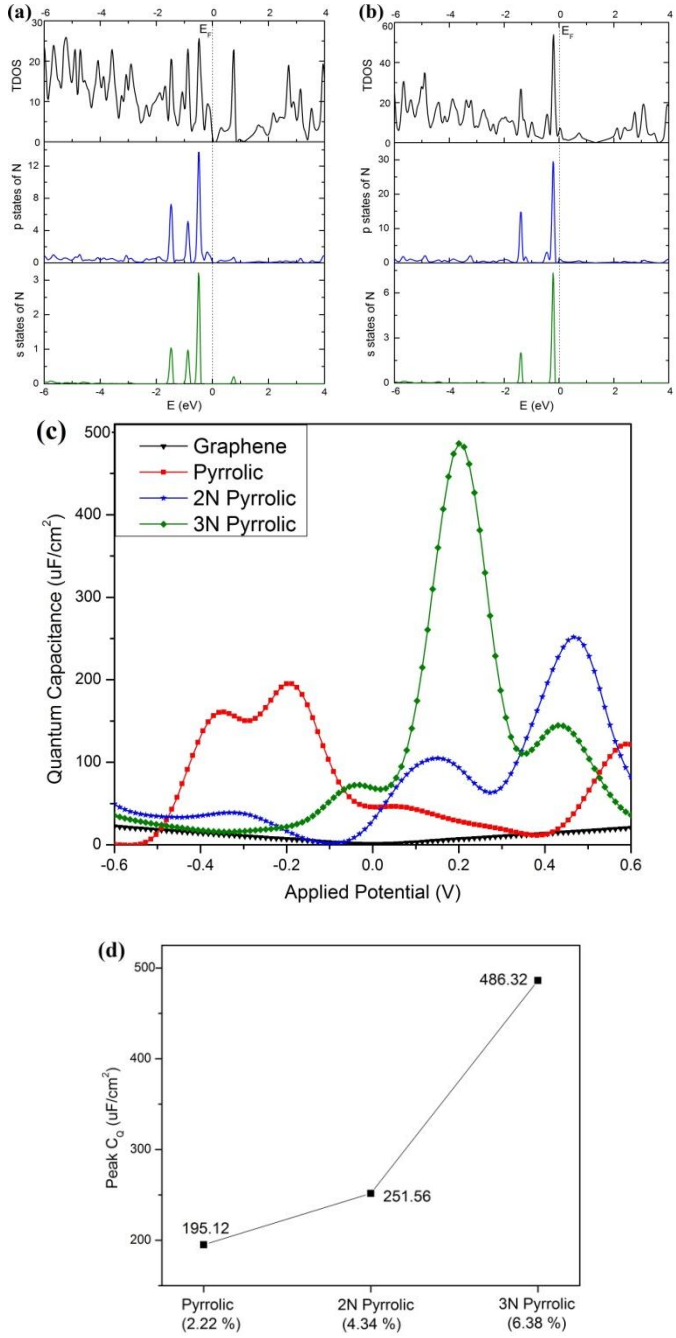

Fig. 4. TDOS and PDOS for (a) 2N pyrrolic, (b) 3N pyrrolic graphenes (Fermi level (E_F) is located at energy zero, DOS are in the units of eV^{-1}). (c) Quantum Capacitance plotted as a function of applied potential, (d) peak value of quantum capacitance, for increasing pyrrolic concentrations.

Here, g_s and g_v are spin and valley degeneracies (=2), respectively. ħ is the reduced planck's constant, v_F is the Fermi velocity of graphene carriers (~ 10^8 cm/s), and E refers to energy. As seen from Fig.(2), our DFT based TDOS for pristine graphene is in reasonable agreement with the TDOS plotted from eq-(2).

The TDOS and PDOS for pristine graphene and primary defect configurations are shown in Fig.3. From Fig.3(a), the pristine graphene exhibits a perfect zero band gap at the fermi level. Further, the observed PDOS around the Fermi level are solely from p-states of carbon. This can be explained from the side of graphene chemistry. In graphene, each tetravalent carbon undergoes sp^2 hybridization in order to bond with three neighboring carbons. This results in three sp^2 hybrid orbitals which can accommodate one electron each, and there will be a left over p-orbital (p_z in our case) with occupancy of one electron. Each of these three sp^2 hybrid orbitals form a σ-bond with the sp^2 hybrid orbital of a neighboring carbon, while the leftover out of plane p_z orbital forms a π-bond. This π-bond is highly delocalized in nature and results in conjugation or aromaticity. Conduction in pristine graphene is caused purely by this delocalized π-cloud from p_z-orbitals, hence only p-states are located around the Fermi level in Fig.3(a). Injecting Stone-Wales defect into graphene affected the electronic nature meagerly, with a few defect induced p-states near the Fermi level, as witnessed from Fig.3(b). The graphitic defect has shifted the Fermi level of graphene up into the conduction band, thereby resulting in n-type behavior induced 'meltallic nature'. This shift shown in Fig.3(c) can be attributed to the induced excessive electron on the graphene sheet as the tetravalent carbon is replaced by pentavalent nitrogen during the graphitic defect process. This excessive electron is located in the form of a lone pair (Fig.S1(c) of supporting information gives an idea of lone pair on Nitrogen) in the p_z orbital of nitrogen. Hence, there exist significant p-states of nitrogen at the Fermi level of graphitic defected sheet.

Introducing the pyridinic defect into graphene shifted down the Fermi level into valence band, thereby resulting in p-type behavior induced 'meltallic nature'. This shift can be attributed to the electron deficiency caused by the carbon vacancy. The states induced by the lone pair of pyridinic nitrogen are located in the valence band as observed from PDOS of Fig.3(d). Introducing the pyrrolic defect into graphene also shifted down the Fermi level into valence band, thereby resulting in p-type behavior induced 'meltallic nature'. This shift can also be attributed to the electron deficiency caused by the carbon vacancy. There is a significant contribution of states from the lone pair of nitrogen near the Fermi level, as seen from Fig.3(e). In contrast to graphitic defect, both the pyridinc and pyrrolic defects have significant PDOS from s-states of nitrogen near the Fermi level. Reason being, the presence of a left over (unbonded) sp^2 hybrid orbital on nitrogen, as the dopant is chemically bonded to only two carbons in these cases. The point to be noted from the analysis of electronic properties is the ability of nitrogen based primary defects to induce metallicity in graphene.

To assess the application of defected configurations for supercapacitor electrodes, we have calculated the quantum capacitance from their respective DOS profiles. In general, the quantum capacitance is defined as $C_Q = \frac{dQ}{d\varphi}$, where Q is excessive charge on graphene electrode and φ is external

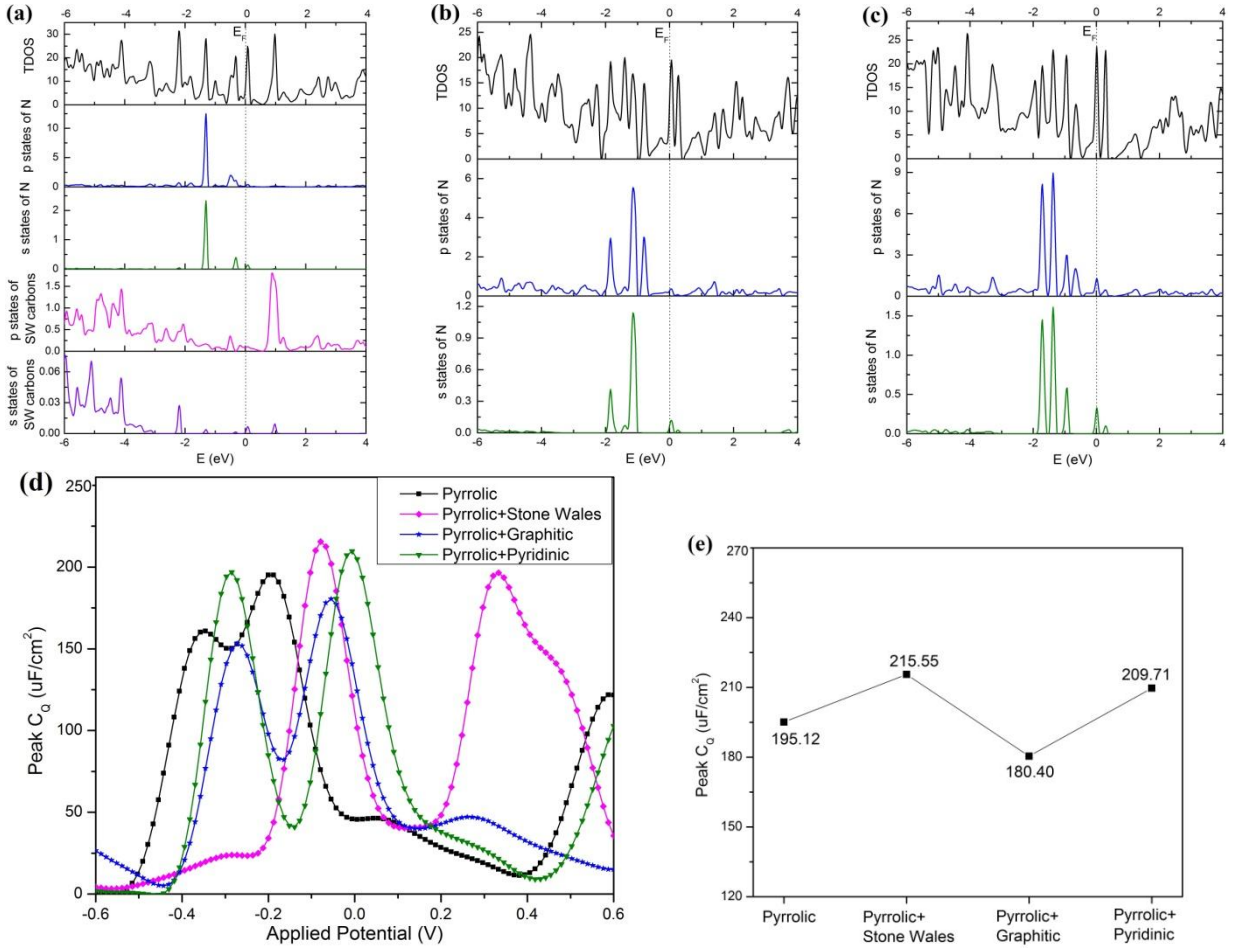

Fig. 5. TDOS and PDOS for combinational pyrrolic defect configurations (a) Pyrrolic + Stone-Wales, (b) Pyrrolic + Graphitic, (c) Pyrrolic + Pyridinic (Fermi level (E_F) is located at energy zero, DOS are in the units of eV^{-1}). (d) Quantum Capacitance plotted as a function of applied potential, (e) peak value of quantum capacitance for the combinational pyrrolic defects.

potential. When the chemical potential of electrons is shifted by applying φ/e, the charge on graphene is [24],

$$Q = e\int_{-\infty}^{\infty} D(E)[f(E) - f(E-\varphi)]\,dE \qquad \text{- (3)}$$

Here, D(E) is the DOS, $f(E)$ is Fermi-Dirac distribution function, E refers to Energy with respect to Fermi level, and e is elementary charge ($1.6*10^{-19}$ C).

By differentiating Q with respect to φ, one can obtain the expression for quantum capacitance as,

$$C_Q = \frac{dQ}{d\varphi} = e^2\int_{-\infty}^{\infty} D(E)[F_T(E-\varphi)]\,dE \qquad \text{- (4)}$$

Here, $F_T(E)$ is the thermal broadening function, given by,

$$F_T(E) = \frac{1}{4KT}sech^2\left(\frac{E}{2KT}\right) \qquad \text{- (5)}$$

By performing the much needed correction inside the hyperbolic secant function for maintaining the charge/discharge synchronization between quantum capacitance and DOS profile, the final expression for C_Q is given as [25],

$$C_Q = \frac{e^2}{4KT}\int_{-\infty}^{\infty} D(E)sech^2\left(\frac{E+\varphi}{2KT}\right)dE \qquad \text{- (6)}$$

Our method of calculating the quantum capacitance follows fixed band approximation, that is the DOS profile of graphene system is assumed to be not affected by charging/discharging. The DOS profiles extracted using Quantum ESPRESSO package have been processed through MATLAB [26] programming to obtain the Quantum Capacitance. The calculated quantum capacitances for pristine graphene and its primary defect configurations are plotted in Fig.3(f) over the applied potential range -0.6 V to 0.6 V (electrochemical range for aqueous electrolytes). Our calculated quantum capacitance for pristine graphene is in excellent agreement with the previous computational reports [24, 25]. It is evident from Fig.3(f), that injecting primary defects into graphene have resulted in clear enhancement in the quantum capacitance over most of the applied potential range. The peak value of C_Q for pristine graphene is measured as 22.17 uF/cm^2 at -0.6 V. While for Stone-Wales defect it is 110.85 uF/cm^2 at -0.41 V, for graphitic defect it is 123.77 uF/cm^2 at -0.54 V, for

pyridinic defect it is 91.39 uF/cm^2 at 0.6 V, and for pyrrolic defect it is 195.12 uF/cm^2 at -0.18 V. The C_Q of graphitic defect (doping concentration of 2%) is in excellent agreement with the previous report [25]. The peak C_Q observed for pristine graphene and its primary defects are listed in table.I and picturized in Fig.3(g), where the peak C_Q follows the trend pyrrolic > graphitic > Stone-Wales > Pyridinic > pristine graphene. Thus, the pyrrolic defect has dominated its counterparts with remarkable 195.12 uF/cm^2 of C_Q, which is a result of enormous peak located at 0.18 eV of TDOS profile. The Stone-Wales, graphitic and pyrrolic defected graphenes offer high quantum capacitances at negative side of the electrochemical window, and hence may be best suitable for cathode electrode of asymmetric supercapacitors. The pyridinic graphene offer peaks in the positive side of the electrochemical window and hence may be best suitable for anode electrode. Considering the remarkable C_Q of pyrrolic graphene, we have proceeded further to analyze the impact of increasing pyrrolic concentration and combinational pyrrolic defects on the graphene sheet.

B. Impact of Pyrrolic Concentration

We have analyzed the impact of increasing pyrrolic defect concentration on the thermodynamic stability, electronic nature and quantum capacitance of graphene. Besides the primary pyrrolic system (2.22 % pyrrolic concentration), we have considered two more systems 2N pyrrolic and 3N pyrrolic with concentration of 4.34 % and 6.38 %, respectively. From table I, the thermodynamic stability assessed from formation energies follow the trend 3N pyrrolic > 2N pyrrolic > pyrrolic, predicting increased thermodynamic stability of graphene with the pyrrolic concentration. From TDOS and PDOS calculations shown in Fig.4(a-b), both the 2N pyrrolic and 3N pyrrolic defects have caused the Fermi level of graphene to shift into valence band, thereby resulting in p-type behavior induced 'meltallic nature'. These shifts can also be attributed to the electron deficiency caused by the carbon vacancies. A significant contribution to PDOS near the Fermi level can be witnessed from s and p-states of nitrogens owing to the presence of lone pairs and unbounded sp^2 hybrid orbitals, one on each of the nitrogen atoms.

The estimated quantum capacitances with increasing pyrrolic defect concentrations are presented in fig.4(c-d), where the pyrrolic systems retained higher quantum capacitance than pristine graphene over the most of electrochemical range. Further, a substantial increase in the quantum capacitance has been witnessed when the doping concentration is increased from 4.34 % (2N pyrrolic) to 6.38 % (3N pyrrolic). This substantial rise in C_Q of 3N pyrrolic system can be related to the enormous peak observed in the TDOS profile at -0.2 eV. A peak C_Q of 195.12 uF/cm^2 has been measured for pyrrolic system at -0.18 V, while it is 251.56 uF/cm^2 at 0.46 V for 2N pyrrolic, and 486.32 uF/cm^2 at 0.2 V for 3N pyrrolic systems. It has been noted that, the peak C_Q increases with the pyrrolic defect concentration. Moreover, the 2N and 3N pyrrolic systems offer remarkable C_Q peaks at the positive side of electrochemical window, asserting their best suitability for anode electrodes of supercapacitors. With a view to assess the impact of other primary defects on the pyrrolic systems, we proceed to study the combinational pyrrolic defects on graphene.

C. Combinational Pyrrolic Defects

The primary defects such as Stone-Wales, graphitic and pyridinic are imposed onto the pyrrolic system as shown in Fig.1(h-j) to form combinational pyrrolic defects. The thermodynamic stability analysis from table.I reveal the reduced stability of pyrrolic system after imposing Stone-Wales and graphitic defects. Where, the graphitic defect causes less degradation of stability of pyrrolic system in comparison to Stone-Wales defect. Reason being the least formation energy of simple graphitic defect on pristine graphene, as witnessed earlier in 'primary defects' section. Surprisingly, imposing pyridinic defect on the pyrrolic system has resulted in improved thermodynamic stability, despite the large formation energy of simple pyridinic defect on pristine graphene. This stability enhancement can be attributed to the reduced dangling carbons at the vacancy defect site of pyrrolic + pyridinic system. The stability of the combinational pyrrolic systems follows the pattern pyrrolic + pyridinic > pyrrolic > Pyrrolic + graphitic > Pyrrolic + Stone-Wales. As witnessed from Fig.5(a-c), the electron deficiency caused Fermi level shift into valence band articulates the p-type behaviour induced 'metallic nature' of combinational pyrrolic systems. The calculated quantum capacitances for the combinational pyrrolic defects are plotted in Fig.5(d-e) in reference with the pyrrolic defect. The primary defects have minimal impact on the peak C_Q of pyrrolic system. Injecting the graphitic defect onto pyrrolic system reduced the peak C_Q by 7.54 %, while Stone-Wales and pyridinic defects resulted in enhancement of peak C_Q by 10.47 % and 7.47 %, respectively. For pyrrolic + graphitic case the measured peak C_Q is 180.40 uF/cm^2 at -0.05 V, while it is 209.71 uF/cm^2 at 0 V for pyrrolic + pyridinic case, and 215.55 uF/cm^2 at -0.07 V for pyrrolic + Stone-Wales case. The measured peak C_Q of the combinational pyrrolic defects follows the pattern pyrrolic + Stone-Wales > pyrrolic + pyridinic > pyrrolic > pyrrolic + graphitic.

To summarize, the pyrrolic defect is observed to be more favorable than other primary defects with respect to the quantum capacitance. In addition, the quantum capacitance is observed to increase with the pyrrolic concentration. Our results dictate that, even if the Stone-Wales, graphitic and pyridinic defects are generated mistakenly alongside the pyrrolic defects during creation process, their impact will be minimal. Though the pyrrolic systems offer less relative thermodynamic stability in comparison to other primary defects owing to their relatively higher formation energies; it may be least of the concerns. Since, the relative high formation energies of pyrrolic systems are a result of large

vacancy defect (diameter ~ 6Å) on which they were implemented. As reported elsewhere [15], a vacancy defect of this size (~ 6Å) helps improve the double layer capacitance at electrode surface by facilitating efficient electrolyte wettability and rate capability. Further, the formation energy reduces (stability increases) with increasing pyrrolic concentration, thus the stability issue can be avoided by preparing pyrrolic rich graphenes. Our computational results presented in this work provide more qualitative view of the pyrrolic rich graphenes rather than quantitative, however, for quantitative confirmation of quantum capacitances for these systems experimental evaluation may be needed.

IV. CONCLUSION

The present work explores a way of enhancing the energy density of graphene supercapacitors by improving the quantum capacitance of grapehene sheets. We used pyrrolic type nitrogen doping to demonstrate extremely high quantum capacitances for graphene. Our plane wave DFT results suggest that, pyrrolic defect configuration can offer much higher quantum capacitance than Stone-Wales, graphitic and pyridinic type defects. Further, the quantum capacitance of graphene is observed to increase with the injected pyrrolic concentration. An extremely high quantum capacitance of 486.32 uF/cm^2 has been witnessed at a pyrrolic concentration of 6.38%. We have also studied the combinational pyrrolic defects to assess the impact of other defects on pyrrolic graphene, and witnessed negligible impact by Stone-Wales, graphitic and pyridinic defects. It is our strong belief that the pyrrolic rich graphenes are an excellent choice for design of high energy density supercapacitors.

SUPPORTING INFORMATION

Electron density plots for different graphene configurations giving an idea of presence of lone pair on Nitrogen are presented in the supporting information.

ACKNOWLEDGEMENT

The authors are thankful to National PARAM Supercomputing Facility (NPSF) at CDAC, India for computational facility and ABV - Indian Institute of Information Technology and Management, and Michigan Technological University for providing the infrastructural support for carrying out this research work. They would also like to thank Prof. De-en Jiang and Cheng Zhan of University of California, Riverside for the valuable scientific discussions.

REFERENCES

[1] Bayani, Amir Hossein, Daryoosh Dideban, and Negin Moezi. "Hydrogen sensitive field-effect transistor based on germanene nanoribbon and optical properties of hydrogenated germanene." *Journal of Computational Electronics* 15, no. 2 (Jun 2016): 381-388.

[2] Bayani, Amir Hossein, Nasser Shahtahmassebi, and Davoud Vahedi Fakhrabad. "The study of the effect of increasing adsorbed hydrogen's atomic percentage on electronic properties of boron-nitride nanotube." *Physica E: Low-dimensional Systems and Nanostructures* 53 (Sep 2013): 168-172.

[3] Khan, Md Shahzad, and Mohd Shahid Khan. "Transition metal decorated borazine complex for hydrogen storage and unfavourable consequence of spin shift for hydrogen storage on Ti-decorated borazine: A DFT study." *Vacuum* 101 (Mar 2014): 151-156.

[4] Zhan, Cheng, Cheng Lian, Yu Zhang, Matthew W. Thompson, Yu Xie, Jianzhong Wu, Paul RC Kent, Peter T. Cummings, De-en Jiang, and David J. Wesolowski. "Computational Insights into Materials and Interfaces for Capacitive Energy Storage." *Advanced Science* (Apr 2017), DOI: 10.1002/advs.201700059.

[5] Liu, Chenguang, Zhenning Yu, David Neff, Aruna Zhamu, and Bor Z. Jang. "Graphene-based supercapacitor with an ultrahigh energy density." *Nano letters* 10, no. 12 (Nov 2010): 4863-4868.

[6] Paek, Eunsu, Alexander J. Pak, and Gyeong S. Hwang. "A computational study of the interfacial structure and capacitance of graphene in [BMIM][PF6] ionic liquid." *Journal of The Electrochemical Society* 160, no. 1 (Jan 2013): A1-A10.

[7] Taluja, Yogita, Boddepalli SanthiBhushan, Shekhar Yadav, and Anurag Srivastava. "Defect and functionalized graphene for supercapacitor electrodes." *Superlattices and Microstructures* 98 (Oct 2016): 306-315.

[8] Jeong, Hyung Mo, Jung Woo Lee, Weon Ho Shin, Yoon Jeong Choi, Hyun Joon Shin, Jeung Ku Kang, and Jang Wook Choi. "Nitrogen-doped graphene for high-performance ultracapacitors and the importance of nitrogen-doped sites at basal planes." *Nano letters* 11, no. 6 (May 2011): 2472-2477.

[9] Zhu, Jingyi, Anthony S. Childress, Mehmet Karakaya, Sushmita Dandeliya, Anurag Srivastava, Ye Lin, Apparao M. Rao, and Ramakrishna Podila. "Defect-Engineered Graphene for High-Energy-and High-Power-Density Supercapacitor Devices." *Advanced Materials* 28, no. 33 (Sep 2016): 7185-7192.

[10] Hirunsit, Pussana, Monrudee Liangruksa, and Paisan Khanchaitit. "Electronic structures and quantum capacitance of monolayer and multilayer graphenes influenced by Al, B, N and P doping, and monovacancy: Theoretical study." *Carbon* 108 (Nov 2016): 7-20.

[11] Paek, Eunsu, Alexander J. Pak, Kyoung E. Kweon, and Gyeong S. Hwang. "On the origin of the enhanced supercapacitor performance of nitrogen-doped graphene." *The Journal of Physical Chemistry C* 117, no. 11 (May 2013): 5610-5616.

[12] Mousavi-Khoshdel, Morteza, Ehsan Targholi, and Mohammad J. Momeni. "First-Principles Calculation of Quantum Capacitance of Codoped Graphenes as Supercapacitor Electrodes." *The Journal of Physical Chemistry C* 119, no. 47 (Nov 2015): 26290-26295.

[13] Wood, Brandon C., Tadashi Ogitsu, Minoru Otani, and Juergen Biener. "First-principles-inspired design strategies for graphene-based supercapacitor electrodes." *The Journal of Physical Chemistry C* 118, no. 1 (Dec 2013): 4-15.

[14] Yang, G. M., H. Z. Zhang, X. F. Fan, and W. T. Zheng. "Density functional theory calculations for the quantum capacitance performance of graphene-based electrode material." *The Journal of Physical Chemistry C* 119, no. 12 (Mar 2015): 6464-6470.

[15] Luo, Gaixia, Lizhao Liu, Junfeng Zhang, Guobao Li, Baolin Wang, and Jijun Zhao. "Hole defects and nitrogen doping in graphene: implication for supercapacitor applications." *ACS applied materials & interfaces* 5, no. 21 (Oct 2013): 11184-11193.

[16] Zhao, Yufeng, Shifei Huang, Meirong Xia, Sarish Rehman, Shichun Mu, Zongkui Kou, Zhi Zhang, Zhaoyang Chen, Faming Gao, and Yanglong Hou. "NPO co-doped high performance 3D graphene prepared through red phosphorous-assisted "cutting-thin" technique: A universal synthesis and multifunctional applications." *Nano Energy* 28 (Oct 2016): 346-355.

[17] Giannozzi, Paolo, Stefano Baroni, Nicola Bonini, Matteo Calandra, Roberto Car, Carlo Cavazzoni, Davide Ceresoli et al. "QUANTUM ESPRESSO: a modular and open-source software project for quantum simulations of materials." *Journal of physics: Condensed matter* 21, no. 39 (Sep 2009): 395502; http://www.quantum-espresso.org/

[18] Garrity, Kevin F., Joseph W. Bennett, Karin M. Rabe, and David Vanderbilt. "Pseudopotentials for high-throughput DFT calculations." *Computational Materials Science* 81 (Jan. 2014): 446-452.

[19] Perdew, John P., Kieron Burke, and Matthias Ernzerhof. "Generalized gradient approximation made simple." *Physical review letters* 77, no. 18 (Oct 1996): 3865.
[20] Marzari, Nicola, David Vanderbilt, Alessandro De Vita, and M. C. Payne. "Thermal contraction and disordering of the Al (110) surface." *Physical review letters* 82, no. 16 (Apr 1999): 3296.
[21] Fasolino, Annalisa, J. H. Los, and Mikhail I. Katsnelson. "Intrinsic ripples in graphene." *Nature materials* 6, no. 11 (Nov 2007): 858-861.
[22] Warner, Jamie H., Gun-Do Lee, Kuang He, Alex W. Robertson, Euijoon Yoon, and Angus I. Kirkland. "Bond length and charge density variations within extended arm chair defects in graphene." *ACS nano* 7, no. 11 (Oct 2013): 9860-9866.
[23] Fang, Tian, Aniruddha Konar, Huili Xing, and Debdeep Jena. "Carrier statistics and quantum capacitance of graphene sheets and ribbons." *Applied Physics Letters* 91, no. 9 (Aug 2007): 092109.
[24] Zhan, Cheng, Justin Neal, Jianzhong Wu, and De-en Jiang. "Quantum effects on the capacitance of graphene-based electrodes." *The Journal of Physical Chemistry C* 119, no. 39 (Sep 2015): 22297-22303.
[25] Zhan, Cheng, Yu Zhang, Peter T. Cummings, and De-en Jiang. "Enhancing graphene capacitance by nitrogen: effects of doping configuration and concentration." *Physical Chemistry Chemical Physics* 18, no. 6 (Jan 2016): 4668-4674.
[26] Matrix Laboratory (MATLAB), accessed on Nov. 15, 2017. [Online]. Available: https://mathworks.com/

Boddepalli SanthiBhushan (S'16) received the bachelor's degree from Jawaharlal Nehru Technological University, Kakinada, India, in 2010, and the M.Tech. degree from the Atal Bihari Vajpayee–Indian Institute of Information Technology and Management, Gwalior, India, in 2013, where he is currently pursuing the Ph.D. degree.

His current research interests include supercapacitors, single electron devices and nanoelectronics.

Mohammad Shahzad Khan received the master's and Ph.D. degrees in physics from Jamia Millia Islamia, A Central University, New Delhi, India, in 2008 and 2014, respectively.

He worked as a visiting Post-Doctoral researcher at Michigan Technological University, USA. He is is currently a Post-Doctoral Researcher at Atal Bihari Vajpayee–Indian Institute of Information Technology and Management, Gwalior, India. His current research interests include modeling and simulation of novel nanomaterials.

Vijay Kumar Bohat (S'17) received the bachelor's degree from Jabalpur Engineering College, Jabalpur, India, in 2010, and the M.Tech. degree from the Atal Bihari Vajpayee–Indian Institute of Information Technology and Management, Gwalior, India, in 2012, where he is currently pursuing the Ph.D. degree.

His current research interests include swarm intelligence, optimization and image processing.

Anurag Srivastava (M'16) received the Ph.D. degree in physics from Barkatullah University, Bhopal, India, in 1998. He worked as a post doctoral researcher at Uppsala University, Uppsala, Sweden, under the supervision of Prof. B. Johansson and Prof. R. Ahuja.

He is currently an Associate Professor with the Atal Bihari Vajpayee–Indian Institute of Information Technology and Management, Gwalior, India. His current research interests include computational materials science and nanoelectronics.